Journal of Magnetic Resonance 201 (2009) 48–56

Contents lists available at ScienceDirect

Journal of Magnetic Resonance

journal homepage: www.elsevier.com/locate/jmr

A pulsed EPR method to determine distances between paramagnetic centers with strong spectral anisotropy and radicals: The dead-time free RIDME sequence

Sergey Milikisyants [a], Francesco Scarpelli [a], Michelina G. Finiguerra [a,b], Marcellus Ubbink [b], Martina Huber [a,*]

[a] Department of Molecular Physics, Huygens Laboratory, Leiden University, P.O. Box 9504, 2300 RA Leiden, The Netherlands
[b] Leiden Institute of Chemistry, Leiden University, Gorlaeus Laboratories, P.O. Box 9502, 2300 RA Leiden, The Netherlands

ARTICLE INFO

Article history:
Received 22 January 2009
Revised 15 July 2009
Available online 15 August 2009

Keywords:
Pulsed EPR
Distance determination
Transition-metal ion centers
RIDME

ABSTRACT

Methods to determine distances between paramagnetic metal centers and radicals are scarce. This is unfortunate because paramagnetic metal centers are frequent in biological systems and so far have not been employed much as distance markers. Successful pulse sequences that directly target the dipolar interactions cannot be applied to paramagnetic metal centers with fast relaxation rates and large *g*-anisotropy, if no echos can be detected and the excitation bandwidth is not sufficient to cover a sufficiently large part of the spectrum. The RIDME method Kulik et al. (2002) [20] circumvents this problem by making use of the T_1-induced spin-flip of the transition-metal ion. Designed to measure distance between such a fast relaxing metal center and a radical, it suffers from a dead time problem. We show that this is severe because the anisotropy of the metal center broadens the dipolar curves, which therefore, only can be analyzed if the full curve is known. Here, we introduce five-pulse RIDME (5p-RIDME) that is intrinsically dead-time free. Proper functioning of the sequence is demonstrated on a nitroxide biradical. The distance between a low-spin Fe(III) center and a spin label in spin-labeled cytochrome *f* shows the complete dipolar trace of a transition-metal ion center and a spin label, yielding the distance expected from the structure.

1. Introduction

Pulsed EPR has taken a leap forward as a method for structure determination in disordered chemical and biological systems ever since pulsed EPR methods had been developed that directly and selectively probe the dipolar interaction between electron spins [1–3]. Amongst them are 2 + 1 methods and DEER [4–6], solid-echo type single-frequency techniques for refocusing dipolar couplings (SIFTER) [7], and double quantum coherence methods (DQM) [5,6,8]. These techniques are optimized for systems with low spectral anisotropy, such as nitroxide-type spin labels and organic radicals, and require the excitation of a significant part of the spectrum. The spectral widths of the EPR transitions of nitroxides and organic radicals are in the order of several mT at the conventional operating frequency of 9 GHz (X-band EPR), which compares well with presently available excitation bandwidths of a few mT (e.g. a pulse length of 24 ns results in 1.5 mT bandwidth). For transition-metal ions, the spectral width is usually larger. Examples for transition-metal DEER refer to those transition-metal ions that have moderate spectral anisotropies, such as Cu(II), where *g*-values between 2.37 and 2.08 give rise to spectral widths of 70 mT at X-band EPR, [9–12] or iron–sulfur centers [13]. Most other transition-metal ions have larger *g*-anisotropies and faster relaxation times even at cryogenic temperatures. For those metal ions, fractional excitation of the spectrum or short relaxation times will either severely limit the sensitivity or make the application of the method impossible. Therefore, novel approaches to address such paramagnetic centers are sought. The present account describes a method tailored to determine the interaction between a low *g*-anisotropy center and a center of large *g*-anisotropy and is ideally suited to address the distance between a nitroxide spin label and a paramagnetic transition-metal ion. For structure determination this combination is highly relevant, because transition-metal centers are often present in proteins. Another advantage of such centers is that they are firmly anchored in the protein and therefore, are not fraught with the problem of flexible linkers as the commonly used spin labels. Previously, most approaches to measure such distances made use of the change in relaxation properties of the small *g*-anisotropy center caused by the transition-metal ion, as pioneered by the group of G. Eaton and S.S. Eaton [14–16]. The approach was used in several recent applications [17,18] and its implementation to obtain long-range distance determination using rare-earth metal ions was described [19]. Nevertheless, the complexity of relaxation-based approaches from the point of view of experiment, but most of all interpretation has so far limited the applications.

The method proposed here directly probes the dipolar interaction between the metal center and a nitroxide or an organic radical. It is based on the relaxation induced dipolar modulation (RIDME)

* Corresponding author. Fax: +31 715275819.
E-mail address: mhuber@molphys.leidenuniv.nl (M. Huber).

1090-7807/$ - see front matter © 2009 Published by Elsevier Inc.
doi:10.1016/j.jmr.2009.08.008

method suggested by Kulik et al. [20], in which the change is detected in the resonance frequency of the observed spin, i.e. the nitroxide (*A*-spin), by the spontaneous flip of the electron spin on the partner paramagnetic center (*B*-spin). Here, the flip of the *B*-spins is not induced by a pump pulse as in traditional sequences, but is left to the longitudinal relaxation of the *B*-spin. As a consequence, there is no need to flip the *B*-spin by a pump pulse, avoiding the problem of the limited excitation bandwidth. The RIDME sequence as proposed originally [20] (Fig. 1a) and the four-pulse version suggested subsequently [21], suffer from a dead time problem that severely limits the usefulness of these methods for distance determination involving systems with high *g*-anisotropy, as we will demonstrate.

We propose a five-pulse version of the RIDME sequence that completely eliminates the dead time. We demonstrate that the sequence works and that it yields the expected distances on a nitroxide biradical (PH2, see Fig. 2) by comparing the results of the new RIDME sequence and a conventional DEER experiment. Subsequently, we apply the new sequence to measure the distance between the low-spin heme iron(III) center, a paramagnetic center with large *g*-anisotropy, and a nitroxide spin label in cytochrome *f* (cyt *f*). This protein is part of the electron transfer chain in photosynthesis and contains an intrinsic low-spin heme Fe(III) center. By site-directed mutagenesis, a cystein was introduced at position 104 and a spin label was attached, resulting in a system with a nitroxide–Fe(III) distance in the order of 1.43 nm. We show that in spite of the large *g*-anisotropy of the Fe(III) center, the distance between the two paramagnetic centers can be determined. A Gaussian distance distribution centered at 1.81 nm with a width of 0.27 nm is obtained. Presently, there is no other method to determine distances in such cases with similar accuracy.

2. Experimental

2.1. Sample preparation

Mutagenesis. The pEAF-wt [22] expression plasmid containing the sequence encoding the soluble domain of cyt *f* from *Nostoc* sp. PCC7119 has been kindly provided by the group of Prof. Miguel

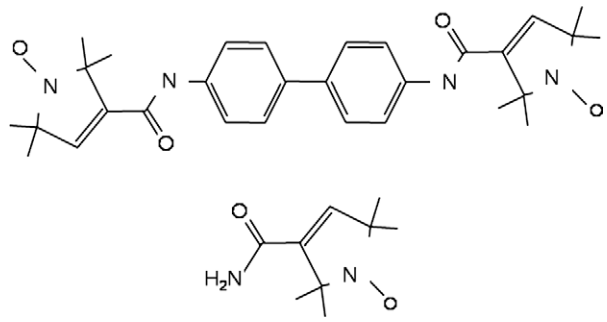

Fig. 2. Chemical structures of the biradical PH2 and the monoradical PH0.

De la Rosa, Instituto de Bioquímica Vegetal y Fotosíntesis, Universidad de Sevilla, Spain. In order to prepare the single-cysteine cyt *f* variants Q104C and N71C, mutations were introduced by site-directed mutagenesis using the Quik Change™ polymerase chain reaction protocol (Stragene, La Jolla, CA) with the plasmid pEAF-wt as a template. To introduce a cysteine instead of the asparagines at the position 71 the direct primer GGCTC***C***AAGGTCGGCTTA ***TG***CGTCGGTGCTG (31 bases) was designed from the nucleotide sequence, inserting at the same time the Sty I restriction site next to the 5′ end of the leader of this primer. Analogously, to introduce a cysteine instead of the glutamine at the position 104 the direct primer CGGCGATGTTTACTTC***TGC***CCCTACGGCGAAG (32 bases) was designed, inserting an extra Bgl I restriction site respect to the *wild type*. Both constructs were verified by DNA sequencing.

2.2. Expression and purification of the cyt f mutants

To improve the maturation and correct insertion of the heme group, *Escherichia coli* strain MV1190 cells (Bio-Rad) were co-transformed with plasmids pEC86 [22] and the cyt *f* expression plasmids. The cells were incubated on Luria–Bertani (LB) medium plates (added by 20 mg/L ampicillin, 20 mg/L chloramphenicol) at 37 °C for 24 h. Several pre-cultures were incubated in 100 mL flasks with 20 mL of LB medium supplemented with 20 mg/L ampicillin (amp) and 20 mg/L chloramphenicol (cam) at 37 °C and

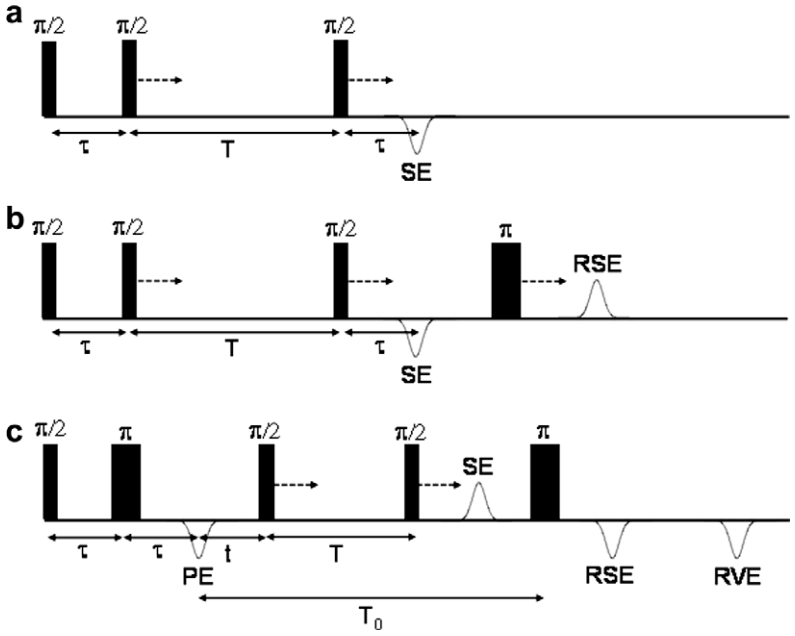

Fig. 1. Pulse sequences for RIDME experiment: (a) three-pulse RIDME and (b) four-pulse RIDME, τ is incremented; (c) five-pulse RIDME, time t is incremented and echo is detected as a function of t. Positions of primary (PE), stimulated (SE), refocused stimulated (RSE) and refocused virtual (RVE) echoes are shown.

250 rpm for 5–6 h. The pre-cultures with the best OD_{600} were used to inoculate 1.7 L (in 5 L Erlenmeyer flasks) in the same medium and incubated at 25 °C and 150 rpm for >72 h under semi-anaerobic conditions and high antibiotics pressure by adding further amp and cam after 20 and 40 h. Induction was achieved 20 h after the inoculation of the large culture using 1 mM IPTG. More than 80 h from the induction the cultures appeared brown for the presence of the cyt; the cells were harvested by centrifugation and the periplasmic fraction was extracted by osmotic shock. The pink water fraction was dialyzed against 2 L of 5 mM Tris–HCl buffer, pH 8 and 3 mM dithiothreitol (DDT). The yield in the periplasmatic fraction was 10 mg/L of protein for N71C and 5 mg/L of Q104C. The resulting dialysate was cleared by centrifugation and loaded onto a DEAE column equilibrated with 5 mM Tris–HCl buffer, pH 8 and 3 mM DDT. Elution has been performed with a gradient of 20–500 mM NaCl and 3 mM DTT. The fractions containing the cyt *f* were concentrated and loaded onto a gel-filtration (G75 Superdex) column and eluted with 5 mM Tris–HCl buffer pH 8, 3 mM DTT and 150 mM NaCl. The fractions containing the protein were pooled, concentrated, dialysed against 5 mM Mes pH 6 and 3 mM DTT and loaded onto a DEAE column equilibrate with 5 mM Mes pH 6 and 3 mM DTT. The protein was eluted with a gradient 0–500 mM NaCl and tested for its purity using the A_{280}/A_{556} ratio. The pure fractions show an A_{280}/A_{556} value of 1.3 under reducing conditions.

2.3. Spin labelling

Before adding the spin label the excess of DTT has been removed from the purified cyt *f* cysteine mutant solution, by several concentration/redilution cycles with degassed 10 mM Na phosphate at pH 6. To avoid reduction of the disulfide by the Fe(II) and concomitant loss of the spin label, a 100-fold excess of $K_3[Fe(CN)_6]$ was added to the solution before adding a 10-fold excess of MTSL [(1-oxyl-2,2,5,5,-tetramethyl-3-pyrroline-3-methyl)-methanethiosulfonate] (purchased from Toronto Research Chemicals, Ont., Canada). The solution was left at 2 h at room temperature and overnight at 4 °C; the excess of $K_3[Fe(CN)_6]$ and MTSL were removed by several concentration/redilution cycles with degassed 10 mM Na phosphate at pH 6.

2.4. Pulsed EPR measurements

All measurements were done on a Bruker E680 ElexSys spectrometer equipped with an ER 4118X-MS3 split-ring resonator of the FlexLine series and an Oxford cryostat. Initial pulse positions for the five-pulse RIDME sequence were 0, 500, 960, $T + 960$ ns, $T + X$ (for T values see text below), X was 2000 ns for nitroxide biradical and 1800 ns for spin labeled cyt *f*. Detector integration gate was 20 ns. Positions of the third and the fourth pulses were incremented with a step of 4 ns, while positions of the other pulses as well as detection gate were not changed.

2.5. Measurements on nitroxides

All experiments on nitroxide solutions were done at 40 K with a repetition time of 10 ms. Pulse lengths for the RIDME experiments were 24 ns and 48 ns for $\frac{\pi}{2}$- and π-pulses, respectively, to compromise between broad excitation bandwidth required to cover spectrally dipolar dublets and sufficiently narrow bandwidth needed to avoid the simultaneous excitation of both spins in the radical couple. All RIDME measurements were done at magnetic field value of 332.75 mT and microwave frequency of 9.372 GHz.

For better comparison with the RIDME results, in the DEER experiments, the observer pulse lengths were the same as in RIDME case: 24 and 48 ns for $\frac{\pi}{2}$- and π-pulses, respectively. The observer pulses (frequency: 9.332 GHz) were positioned at 0, 500, 1400 ns. The pump pulse with a duration of 24 ns and a frequency of 9.397 GHz was initially positioned at 900 ns and swept with a time-step of 4 ns. The RIDME traces of PH2 are obtained by dividing a trace with a long T (T_L), $T_L = 400$ μs by one with a short T (T_S), $T_S = 10$ μs. The value of the external magnetic field for DEER was 331.3 mT.

2.6. Measurements on spin labeled cytochrome f

All experiments were done at 7 K with a repetition time of approximately 1 s and 2 shots per loop. Applied pulse lengths of 12 and 24 ns for $\frac{\pi}{2}$- and π-pulses, respectively, were the shortest achievable on our spectrometer. The RIDME traces of both systems (Q104C and N71C) were obtained by dividing a trace with $T = 200$ μs (T_L) by one with $T = 5$ μs (T_S). The microwave frequency and magnetic field value were 9.306 GHz and 330.45 mT, respectively.

2.7. Numerical calculations

All numerical calculations were done using the R2006b version of the MATLAB software. To calculate Pake patterns (dipolar frequencies) and the corresponding time traces, we assumed the orientation distributions for *g*-tensor and the inter-radical vector to be isotropic and mutually independent. To avoid numerical singularities for the Pake distributions, we assumed an intrinsic Gaussian line-width of 0.16 MHz.

3. Results and discussion

In the following we first describe the background relevant to the method and introduce the new pulse sequence. Then we report measurements of the nitroxide–nitroxide distance in PH2 and of the distance between a nitroxide spin label and the low-spin Fe(III) center in the cyt *f* mutant.

3.1. Background of the method, dipolar interaction between two electron spins

The magnetic dipole–dipole interaction between two unpaired electron spins (spin 1 and spin 2) is described by the Hamiltonian [23]

$$H_{dd} = \frac{1}{r^3}\left[(\hat{\bar{\mu}}_1 \cdot \hat{\bar{\mu}}_2) - 3\frac{(\hat{\bar{\mu}}_1 \cdot \hat{\bar{r}})(\hat{\bar{\mu}}_2 \cdot \hat{\bar{r}})}{r^2}\right]$$

where $\hat{\bar{\mu}}_1$ and $\hat{\bar{\mu}}_2$ are magnetic moment operators and $\bar{r}$ is the vector connecting the positions of the interacting spins. Our further discussion will be based on the assumption that the electron Zeeman interaction for each of the spins and the difference in their resonance energies are much larger than dipole–dipole interaction between them. In this case, the spin wave functions of each spin can be considered as independent of each other. Then, in first order approximation, the resonance energies are determined only by the Zeeman term. The dipolar interaction can be interpreted as the interaction between the magnetic moment of spin 1 and the magnetic field induced by spin 2 at the position of spin 1 and vice versa. If the *g*-tensor of spin 1 is isotropic, the quantization axis of this spin is coincident with the direction of the external magnetic field. Therefore, the magnetic field ΔB induced by spin 1 at the position of spin 2 can be written in the following form

$$\Delta B = \pm\frac{1}{2}\frac{\mu_0 g_1 \beta_e}{4\pi}\frac{1}{r^3}\left(\frac{\bar{B}}{|B|} - \cos(\theta)\frac{\bar{r}}{|r|}\right) \quad (1)$$

Here g_1 is the *g*-value of spin 1 and θ is the angle between external magnetic field $\bar{B}$ and vector $\bar{r}$. The sign refers to the two quantum states of spin 1. The magnetic field induced by spin 1 has two

components, the first one is along the external magnetic field and the second one is along $\bar{r}$. Our further consideration will be in the reference axes system, where the g-tensor of spin 2 is diagonal, as shown in Fig. 3. In this coordinate system the interaction energy (ω_2) between spin 2 and the external magnetic field B is given by

$$\begin{aligned}\omega_2 &= \frac{\beta_e}{\hbar}\sqrt{(g_{2x}B_x)^2+(g_{2y}B_y)^2+(g_{2z}B_z)^2}\\ &= \frac{\beta_e}{\hbar}\sqrt{(g_{2x}B\sin\theta_B\cos\varphi_B)^2+(g_{2y}B\sin\theta_B\sin\varphi_B)^2+(g_{2z}B\cos\theta_B)^2}\end{aligned} \tag{2}$$

were θ_B and φ_B are the polar angles of the magnetic field direction and g_{2x}, g_{2y}, g_{2z} are the principal values of the g-tensor of spin 2. Adding the magnetic field induced by spin 1 (1) to the external one in the Eq. (2) and using the Taylor series expansion for the square root function in (2) we obtain the first order approximation for the dipolar interaction energy between two spins

$$\begin{aligned}\omega_{dd} = \frac{\mu_0 g_1 \beta_e^2}{4\pi\hbar}\frac{1}{r^3}\frac{1}{g_{2eff}}\{&g_{2x}^2\sin\theta_B\cos\varphi_B(\sin\theta_B\cos\varphi_B\\ &-3\cos\theta\sin\theta_r\cos\varphi_r)+g_{2y}^2\sin\theta_B\sin\varphi_B(\sin\theta_B\sin\varphi_B\\ &-3\cos\theta\sin\theta_r\sin\varphi_r)+g_{2z}^2\cos\theta_B(\cos\theta_B-3\cos\theta\cos\theta_r)\}\end{aligned}$$

where θ_r and φ_r are the polar angles of vector $\bar{r}$ and g_{2eff} is the effective g-value of spin 2 in presence of field B and given by

$$g_{2eff} = \sqrt{(g_{2x}\sin\theta_B\cos\varphi_B)^2+(g_{2y}\sin\theta_B\sin\varphi_B)^2+(g_{2z}\cos\theta_B)^2}$$

Four angles θ_B, φ_B, θ_r, φ_r uniquely determine the dipolar interaction energy. In disordered samples θ_B and φ_B must be considered as independent variables uniformly distributed over all possible values. In the rigid limit, θ_r and φ_r are fixed and determined by the local geometry of the system. In real systems, however, intrinsic flexibility results in a distribution of θ_r and φ_r. In our further discussion we will assume that the orientations of the g-tensor and the vector $\bar{r}$ are not correlated i.e. that θ_r and φ_r are independent variables as well. The angle θ is not an independent variable and must be expressed as follows:

$$\begin{aligned}\cos\theta = &\cos\theta_B\cos\theta_r+\sin\theta_B\sin\theta_r\cos\varphi_B\cos\varphi_r\\ &+\sin\theta_B\sin\theta_r\sin\varphi_B\sin\varphi_r\end{aligned}$$

Typically, for organic radicals such as nitroxides, the g-anisotropy is very small and one simply assumes $g_1 = g_2 = g_e = 2$. In this case, from the angular dependence of ω_{dd}, a Pake pattern results [24] with two symmetric sharp peaks at

$$\omega_{dd}^{\perp} = \pm\frac{\mu_0\beta_e^2}{\pi\hbar}\frac{1}{r^3}$$

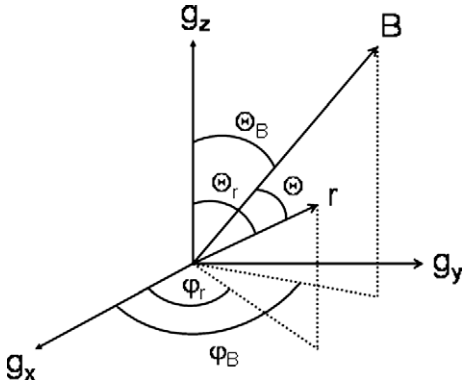

Fig. 3. Reference axes system and definition of angles used in the analysis (see text).

The numerically calculated Pake pattern for an inter-radical distance of 2 nm is shown in Fig. 4a (solid line). It has two sharp peaks at $\omega_{dd}^{\perp}/2\pi$ = ±6.4 MHz. In the time domain, a slowly decaying modulation of the dipolar trace results (solid line, Fig. 4b). For the coupling between an isotropic spin with g = 2 and a spin with a large g-anisotropy (principal values: $g_x = 1, g_y = 2, g_z = 4$), the dashed line in Fig. 4a is obtained The larger g-anisotropy causes a broadening of the Pake pattern. In the time domain (Fig. 4b, dashed line) the signal decays with a characteristic shape until approx. 60 ns, and subsequent modulations are less deep than in the isotropic case.

3.2. The standard RIDME sequence

The pulse sequence for the RIDME experiment is the stimulated echo sequence shown in Fig. 1a. A full analytical description of the method is given in [20]. Here we illustrate the idea of the method with a vector model. The initial magnetization vector in the rotating frame is $\{0, 0, -M_0\}$. After the first $\frac{\pi}{2}$-pulse, which as all following pulses is applied along the x-axis, the magnetization becomes $\{0, -M_0, 0\}$. After a time τ of free evolution the vector is given by $\{-M_0\sin\Omega\tau, -M_0\cos\Omega\tau, 0\}$, where Ω is the off-resonance frequency of the spin packet. The second $\frac{\pi}{2}$-pulse transforms the magnetization vector into $\{-M_0\sin\Omega\tau, 0, M_0\cos\Omega\tau\}$. Under free evolution for a time T that is much larger then the transverse relaxation time T_2, only the z-component survives, resulting in $\{0, 0, M_0\cos\Omega\tau\}$. The immediate result of the third $\frac{\pi}{2}$-pulse is the magnetization vector $\{0, M_0\cos\Omega\tau, 0\}$, which can be presented as the sum of two vectors: $\{-\frac{M_0}{2}\sin\Omega\tau, \frac{M_0}{2}\cos\Omega\tau, 0\}$ and $\{\frac{M_0}{2}\sin\Omega\tau, \frac{M_0}{2}\cos\Omega\tau, 0\}$. The first vector is refocused after a time τ of free evolution resulting in a stimulated echo. The second vector continues defocusing, but it can be refocused by the application of an additional π-pulse resulting in a refocused virtual echo [25]. If during the time T a B-spin, i.e. a spin that has a dipolar interaction with the observed A-spin, flips, the frequency of the A-spin shifts by ω_{dd}, resulting in a modulation of the amplitude for both the stimulated and the virtual echo. By incrementing the time τ in the sequence, this is detected as a cosine function of $\omega_{dd}\tau$. The probability of the flip of the B-spins during the time T is given by

$$\frac{1}{2}\left(1-\exp\left\{-\frac{T}{T_1}\right\}\right) \tag{3}$$

where T_1 is the longitudinal relaxation time of the B-spin. Consequently, T has to be in the order of T_1 and the modulation depth, given by (3), is maximally 0.5 of the echo amplitude.

The original three-pulse RIDME sequence, however, suffers from the dead time problem, i.e. τ cannot be made infinitely small. The experimental inaccessibility of the short τ values, in this case, has two origins. First, resonator ringing prevents echo detection immediately after the third pulse. Second, at τ values comparable with the pulse widths, partial or complete overlap of the first and the second pulse causes distortions of the RIDME trace in exactly the same way as in the basic, three-pulse version of the DEER sequence. The previously proposed four-pulse modification of RIDME with an additional refocusing π-pulse, as shown on Fig. 1b, removes the resonator ringing problem, and reduces the dead time to about 40 ns [21]. Still, the remaining dead time seriously limits the application of the RIDME method to systems where at least one of the coupled spins has a large spectral anisotropy, as discussed in the following.

3.3. Consequences of the dead time for systems with large g-anisotropy

In Fig. 4b, the effect of a large g-anisotropy on the time trace is shown. Whereas for systems with small g-anisotropy the information about the distance between the coupled spins can be obtained

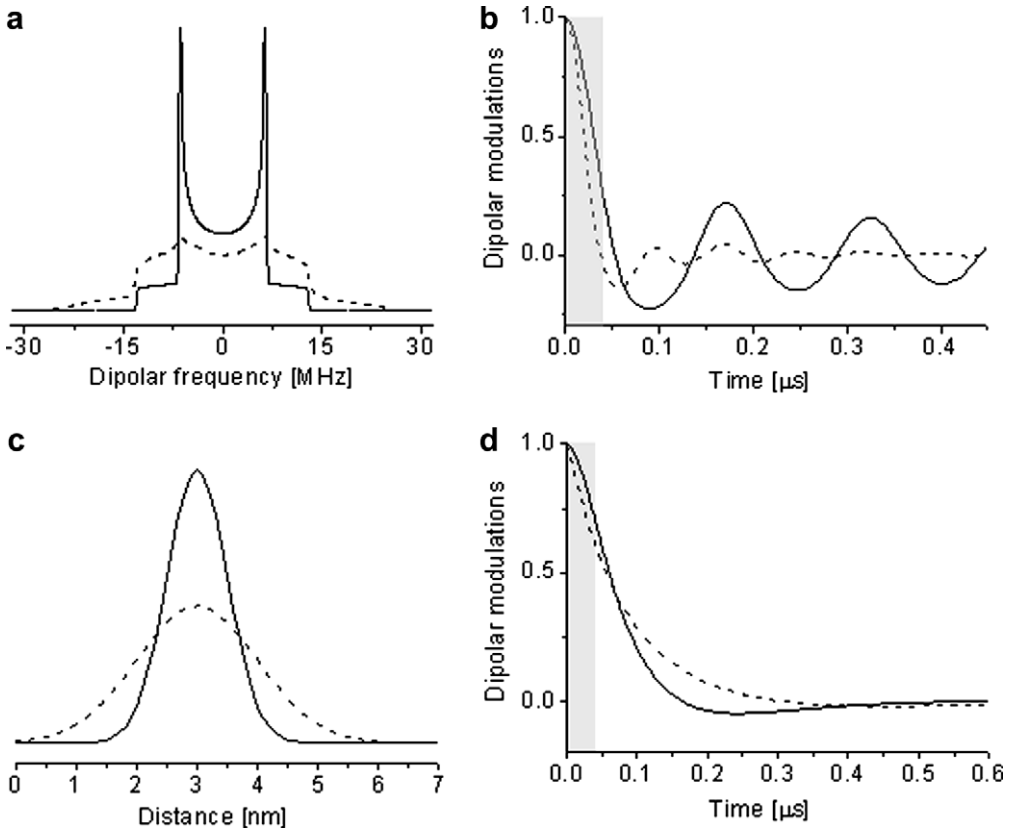

Fig. 4. (a) Pake patterns for isotropic *g*-tensor: solid line, and for rhombic *g*-tensor with $g_x = 1$, $g_y = 2$, $g_z = 4$: dashed line; (b) Corresponding dipolar modulations; (c) two Gaussian distance distribution functions with corresponding dipolar traces in case of *g*-tensor anisotropy with $g_x = 1$, $g_y = 2$, $g_z = 4$. Shadowed bars on figures (b) and (d) indicate the dead time areas of the four-pulse RIDME sequence.

even without taking into account the initial part of the trace, for systems with large *g*-anisotropy the shape of the function (Fig. 4b, dashed line) cannot be reconstructed without measuring the initial part of the trace. This part of the trace is lost in the shaded area that shows the minimal dead time achievable by the traditional RIDME sequences. Fig. 4c and d show the effect of a distribution of distances on the time domain data (Fig. 4d, dashed and solid lines). Distinct time domain traces are obtained, from which the distance distributions can be reconstructed provided that the full trace can be determined experimentally.

3.4. Pulse sequence for dead-time free, five-pulse RIDME

In order to remove the residual dead time an additional π-pulse is introduced into the four-pulse RIDME sequence [20] using a similar approach as was done to develop the four-pulse DEER sequence [26]. The resulting five-pulse RIDME sequence is shown in Fig. 1c. For the detection, one can use either the refocused stimulated (RSE) or the refocused virtual echo (RVE), since both of them are modulated in the same way. Under our experimental conditions, detection on the RVE is better, because it allows to use a shorter phase-evolution (defocusing and refocusing) time to detect a particular time point "*t*" of the dipolar trace than the RSE. This evolution time is approximately 200 ns shorter for the RVE than for the RSE. The evolution times differ for the two echoes because for the detection on the RSE, the instrumental dead time is limited by the ring-down of the resonator (140 ns), whereas for detection on the RVE it is limited by the minimal inter-pulse separation (40 ns). To obtain the shortest phase-evolution time for the RVE the last (fifth) pulse should be positioned 40 ns after the fourth pulse. To do the same for the RSE the position of the fifth pulse must be $t + 140$ ns after the fourth pulse. The amplitude of the RVE is measured as a function of the time delay between the third pulse and the primary echo (PE) created by the first two ($\frac{\pi}{2} - \pi$-) pulses. The positions of the third and the fourth pulse are simultaneously incremented by the same time steps, keeping the time T between them constant. The time interval T_0 between the primary echo and the position of the last pulse must satisfy the condition $T_0 \geqslant T + t_{dip} + t_d$, where t_{dip} is the total length of the dipolar trace to be measured and t_d is dead time needed to avoid that the last two pulses overlap. Since the positions of the first, second and the fifth pulse are kept fixed in time, the total phase-evolution time is constant, avoiding unwanted contributions of T_2 relaxation to the trace.

Although the dead time is eliminated in the same way as in the DEER experiment there is one difference to be considered. At t values close to zero, three echoes, namely the refocused stimulated, the refocused virtual and the primary echo created by the last two pulses of the sequence overlap in time. This distorts the trace at initial times. To remove this problem, phase cycling is required. We use the 8-step phase cycle outlined in Table 1. According to the vector model, the amplitudes of the three echoes depend on the phases of the third (φ_3) and fourth (φ_4) pulse. The refocused virtual echo depends on $e^{i(\varphi_4-\varphi_3)}$, the refocused stimulated echo on $e^{i(\varphi_3+\varphi_4)}$ and the two-pulse echo of the last two pulses in the sequence on $e^{i\varphi_4}$. In principle, the phase cycle $[(+x)+(-x)+(+y)+(-y)]$ on the third and the fourth pulse would be sufficient to eliminate the unwanted echoes. However, if the time T is long, the two refocused echoes can be much smaller in amplitude than the primary echo. In this case, imperfections in the microwave-channel phase adjustment may prevent complete cancellation of the unwanted two-pulse echo. Therefore, an additional two-step

phase cycle $[(+x)-(-x)]$ is applied to the first pulse, to remove remaining distortions from the time trace.

3.5. Suppression of unwanted contributions to the RIDME trace

Additionally to the dipolar modulations, nuclear modulations, spectral diffusion and in principle also orientation exchange by motional processes, e.g. [27] can contribute to the RIDME traces. At the temperatures of the experiments, i.e. at or below 40 K the latter contribution will not play a role, however. The remaining unwanted contributions can be eliminated most reliably by dividing the measured trace by a reference trace of a sample containing only *A*-spins. But even if such a sample is not available, the unwanted contributions can be largely suppressed. As was shown before, [28] nuclear modulations can be suppressed by dividing two traces, one with sufficiently long T (T_L), where the dipolar contribution is substantial, and the other with a much shorter T (T_S) that is still long compared with T_2. In that case, the nuclear modulations should be similar to those in the first trace thus removing the major part of the nuclear modulations. Only nuclear modulation that is dependent on T would remain, but if it is possible to use a T that is longer than decay time of the nuclear coherence even those modulations could be suppressed. Typically the decay time of nuclear coherences is on the time-scale of a few microseconds. This suggests choosing conditions where T_1 for the *B*-spins is much longer than the decay time of nuclear coherence. Thus, by selecting the proper conditions and using proper settings of T_S and T_L for the two traces, nuclear modulation could be largely eliminated. The dipolar contribution would not suffer in this case, since it is present in the trace measured with T_L and not yet developed in the one measured with T_S.

Spectral diffusion in the time interval T, manifests itself in a monotonous decay of the RIDME trace, even though the total echo-refocusing path remains the same. The best experimental conditions for separation of the spectral diffusion component from the dipolar modulations would be to find a parameter T long enough to flip a large fraction of the *B*-spins but still short enough to avoid spectral diffusion. In practice, at least for the experiments discussed here, spectral diffusion components are sufficiently distinct from dipolar modulations that they can be empirically fitted. Spectral diffusion is slowly decaying on the time-scale of the measurement and therefore can be subtracted from the measured curve, whereas nuclear modulation, which is changing rapidly with time, needs to be divided out of the trace.

3.6. Results for the nitroxide biradical

To test the new pulse sequence we used the nitroxide biradical PH2 (Fig. 2), because in this system the distance is well-defined and regular DEER experiments can be performed to verify the RIDME results. In Fig. 5, the DEER results are shown, revealing the regular modulation pattern in the time trace. To provide better comparison with the RIDME results, the timing of the pulses was as in the RIDME experiment and the spectral positions of the observed and pumped spins were chosen as shown on Fig. 5a. For RIDME, the system is not ideal, because the paramagnetic centers, and in particular their T_1 times, are identical. This is not desired, since significant modulation depths can only be obtained if the time T of the RIDME sequence is comparable to or longer than T_1 of the *B*-spins. Here, however, the *A*-spins have the same T_1, making it impossible to detect their signal after such a long T time. Nevertheless, RIDME traces can be obtained as shown in Fig. 5c, solid line. Owing to the small modulation depth for RIDME, nuclear modulations of protons appear alongside the desired electron–electron dipolar modulations. To eliminate the nuclear modulations, the RIDME trace for the PH0 monoradical (dashed line in Fig. 5c) was measured, revealing only nuclear-modulation and spectral-diffusion components. Division of the trace for PH2 by the one for PH0 results in the trace shown in Fig. 5d, in which nuclear modulations and the overall decay of the trace, which is due to spectral diffusion, are absent. The trace is in agreement with the DEER trace, Fig. 5b, showing that the RIDME modulations obtained with the new sequence are indeed caused by the electron–electron spin interaction. The modulation depth is in the order of 15%, i.e. significantly lower than the theoretical maximum of 50%. Given that T is 400 μs and that the T_1 of nitroxides at this temperature is in the ms range, the conditions are far from ideal for efficient RIDME (Eq. (3)), which fully explains the low modulation depth. The dashed line in Fig. 5d shows the fit of the dipolar trace using DeerAnalysis2006 [29–31] with a Gaussian distance distribution at 1.89 and 0.14 nm standard deviation. Faithful reproduction of the experimental curves including the early times confirms that the new RIDME sequence abolishes the dead time and results in the proper shape of the early parts of the curve. The DEER trace, obtained with the same pulse lengths for the observer pulses as the RIDME trace (Fig. 5b) was fitted with parameters of 1.89 nm, and a standard deviation of 0.08 nm. The smaller width of the distribution obtained from DEER reflects the slower decay of the modulation in the DEER experiment. The origin of this difference is not clear at present.

Table 1
Phase cycle used for the 5 pulse RIDME sequence.

φ_1	φ_3	φ_4	Detection
+x	+x	+x	+
+x	−x	−x	+
+x	+y	+y	+
+x	−y	−y	+
−x	+x	+x	−
−x	−x	−x	−
−x	+y	+y	−
−x	−y	−y	−

3.7. Results for spin labeled cytochrome f

The new pulse sequence has been developed for the correlation of a transition-metal ion and a spin label, which we demonstrate for the protein cyt *f* (Q104C), where the spin label interacts with a low-spin Fe(III) center. The RIDME trace for Q104C is shown in Fig. 6a. At times longer than 70 ns, the trace is dominated by the background, which is fitted as a stretched exponential (see Fig. 6a) and subtracted (Fig. 6b). A fast initial decay is observed, but further modulations, as seen in the traces in Fig. 5b and d at times larger than 100 ns, are absent. The dotted line in Fig. 6b shows the fit to the data with low-spin Fe(III) *g*-values of $g_x = 0.9$, $g_y = 1.69$, $g_z = 3.51$ [32], and a Gaussian distance distribution centered at 1.81 nm with a standard deviation of 0.27 nm. The parameters of the distance distribution are only marginally affected by the uncertainty of the g_x value, resulting in variations of about 0.04 nm in the distance and the width for g_x = 0.4, 0.9 or 1.4.

In Fig. 6c, the dependence of the modulation depth on T is shown. For data obtained by dividing a trace with a long T by one with a short T (T_S) (see above) the dependence can be described by a bi-exponential curve according to

$$A = A_0\left[P\left(e^{-\frac{T_S}{T_1^a}} - e^{-\frac{T}{T_1^a}}\right) + (1-P)\left(e^{-\frac{T_S}{T_1^b}} - e^{-\frac{T}{T_1^b}}\right)\right] \quad (4)$$

In the present case, T_S = 5 μs, and T_1^a and T_1^b are the relaxation times of the fast relaxing center. The fraction P refers to the amount of spins relaxing with a time T_1^a and A_0 is the modulation depth

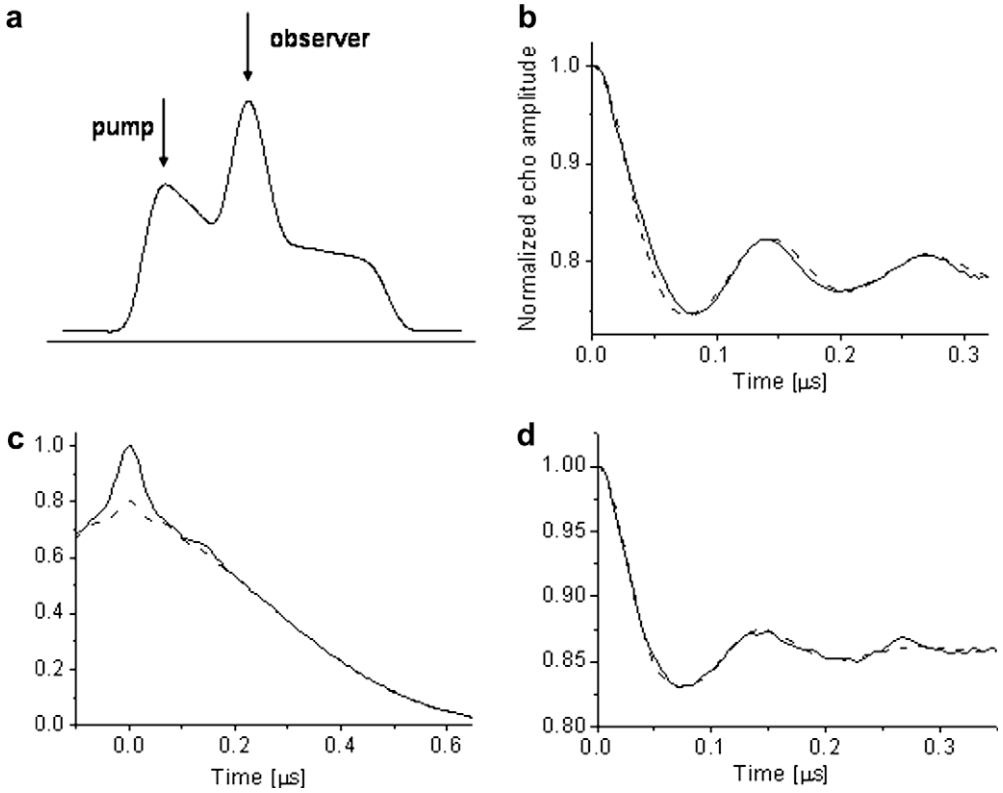

Fig. 5. Experimental data obtained for PH2 biradical. (a) Two-pulse echo detected spectrum Arrow 'pump': spins excited by pump-pulse in DEER; arrow 'observer': spins in DEER and RIDME; (b) DEER trace: solid line and best fit: dashed line; (c) five-pulse RIDME trace for PH2 biradical: solid line, for PH0 monoradical: dashed line, obtained as described in text; (d) dipolar modulations extracted from RIDME traces: solid line, and best fit: dashed line.

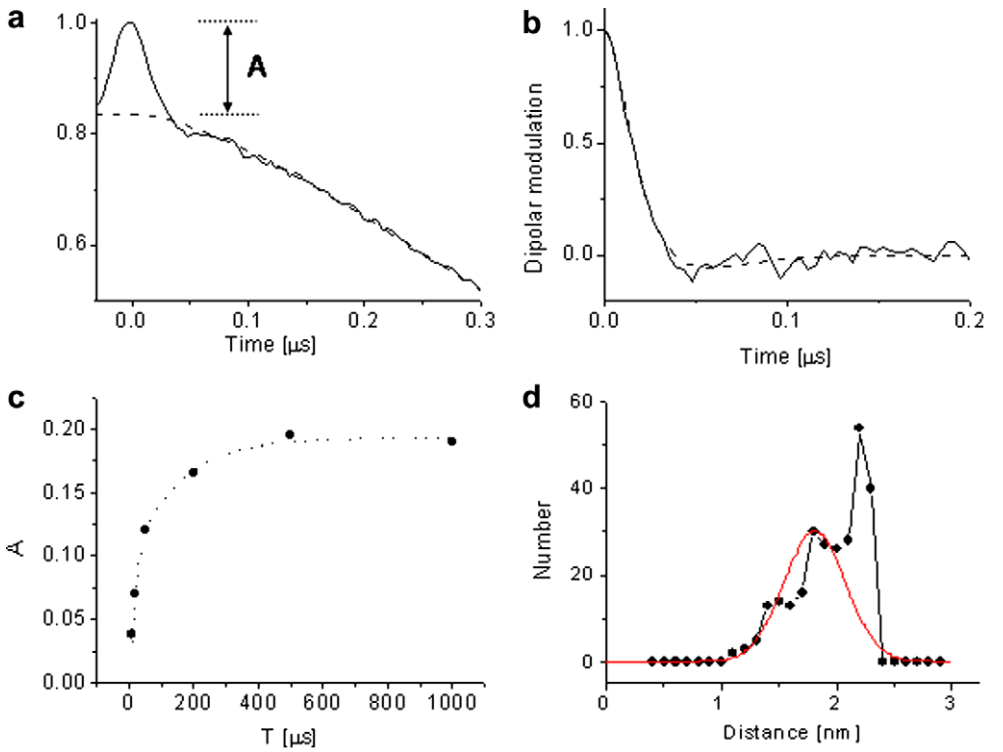

Fig. 6. Results for Q104 mutant of cytochrome *f*. (a) Experimental five-pulse RIDME trace (solid line) obtained as described in the text and stretched exponential fit of the background (dashed line); (b) extracted dipolar modulation contribution (solid line) and its best fit (dashed line); (c) modulation amplitude defined as shown in (a) versus time *T* (points) and the best fit (dashed line). (d) Distance distribution of Q104C mutant (red) superimposed on distance distribution from the model to describe the spin label conformations (dots). (For interpretation of the references to colour in this figure legend, the reader is referred to the web version of this article.)

obtained for an optimal choice of T and T_S. For T_1^a and T_1^b we obtained 13 and 148 μs respectively, which is in good agreement with the values for low-spin iron hemes at this temperature [33]. We attribute the presence of two T_1 times with approximately equal weight ($P = 0.57$) to the anisotropy of the low-spin Fe(III) relaxation times. Anisotropies of similar magnitude were observed for the T_1 times of nitroxide-radical centers [34] suggesting that T_1 anisotropy is a reasonable candidate for the origin of the two T_1 components observed. Also, preliminary measurements on a second mutant (cyt *f* N71C) yielded similar parameters in Eq. (4), emphasizing that the low-spin Fe(III) center is the source of the modulation. The amplitude $A_0 = 0.24$ for Q104C is about half the maximal modulation depth for RIDME, which, according to Eq. (3) is 0.5. The smaller depth found agrees with the fraction of oxidized iron in our samples, which is 56% as determined by optical spectroscopy. Taking this correction into account we conclude that A_0 is 86% of theoretical maximum. This high value also shows that possible distortions due to limited bandwidth of the microwave pulses for such short distances are not significant.

In Table 2, the parameters of the distance distribution are compared to the distances between the iron and the C_β-atoms (Fe-C_β) atoms derived from the X-ray structure of cyt *f*. Given the spin label linker length of 0.5–0.6 nm [8] between the C_β-atom and the center of spin density on the nitroxide, the distance found for Q104C agrees well with the C_β distance from crystallography. Additionally, the conformation of the spin-label linker was modeled [35,36], resulting in the distance distribution shown in Fig. 6d. In this model, all sterically allowed conformations of the spin label linker are taken into account, neglecting specific interactions that the spin label may have with the protein. The resulting distance distributions are expected to be wider than the real distributions. The distance distribution found by RIDME is completely within the range of distances predicted by the model, suggesting a good agreement with the distance between the paramagnetic centers predicted from the model.

We show that the dead-time free RIDME variant can give direct dipolar frequencies and distances between radicals, such as nitroxide spin labels, and transition-metal ions with large *g*-anisotropy and fast relaxation. Distances between radicals and transition-metal ions with smaller g anisotropy, such as Cu(II), can also be measured by DEER and related methods (e.g. [9,11–13]) and in these cases, DEER can be advantageous, given, for example, the potential to provide the relative orientation of the paramagnetic centers (e.g. [11,28,37]). For transition-metal ions that do not exhibit an echo under the usual experimental conditions or that have insufficiently long T_2 times to be used as observer spins, DEER and related methods are not applicable. In these cases, distances derived from the dipolar frequencies obtained from 5p-RIDME are a solution. The method thus extends and complements existing techniques and gives access to a larger range of possible distance markers.

3.8. Summary and outlook

We demonstrate why for a reliable measurement of distances and distance distributions between transition-metal centers and radicals dead-time free dipolar modulation traces are required. The 5p-RIDME sequence introduced here, the dead-time free version of the RIDME method, is designed to do so. Limitations of relaxation times and excitation bandwidths will define the distance ranges accessible, and while it stands to reason that these limits are similar to the DEER method, this will have to be demonstrated on practical examples. We demonstrate the power of the method by the direct measurement in the time domain of the dipolar interaction between a strongly anisotropic low-spin heme iron (III) center and a covalently attached nitroxide spin label in a protein (cyt *f*). We suggest that this technique will open up the way for reliable and selective distance measurements involving paramagnetic metal centers with large spectral anisotropy and fast relaxation.

Table 2
Distance between Fe(III) and spin label in the cyt *f* mutant Q104.

	Distance nm	σ_r nm	FeC_β nm[a]
Q104C	1.81 ± 0.03	0.27 ± 0.08	1.43

[a] From X-ray crystallography, structure pdb-entry 1 TU2.

Acknowledgments

We thank Prof. E.J.J. Groenen for constant interest and support and for crucial comments concerning this manuscript. We thank Prof. Carlo Corvaia for the generous gift of PH2 and PH0 and Dr. Stefano Ceola for discussions and information concerning the biradical and Dr. Alex N. Volkov for simulating the spin-label conformations and for many helpful suggestions concerning spin labeling. Prof. S. Eaton is acknowledged for comments on Fe(III) relaxation. This work is part of the research programme of the 'Stichting voor Fundamenteel Onderzoek der Materie (FOM)', which is financially supported by the 'Nederlandse Organisatie voor Wetenschappelijk Onderzoek (NWO)', Grant 03BMP03. Financial support from NWO (Grants 700.50.026 (MF) and NWO-TOP (FS, MH)) is acknowledged.

References

[1] O. Schiemann, T.F. Prisner, Long-range distance determinations in biomacromolecules by EPR spectroscopy, Quarterly Reviews of Biophysics 40 (2007) 1–53.
[2] P.P. Borbat, J.H. Freed, Measuring distances by pulsed dipolar ESR spectroscopy: spin-labeled histidine kinases, Two-Component Signaling Systems, Pt. B 423 (2007) 52–116.
[3] G. Jeschke, Y. Polyhach, Distance measurements on spin-labelled biomacromolecules by pulsed electron paramagnetic resonance, Physical Chemistry Chemical Physics 9 (2007) 1895–1910.
[4] A.D. Milov, K.M. Salikhov, M.D. Shchirov, Application of the double resonance method to electron spin echo in a study of the spatial distribution of paramagnetic centers in solids, Soviet Physics Solid State (Fizika Tverdogo Tela) 23 (1981) 565–569.
[5] S. Saxena, J.H. Freed, Double quantum two-dimensional Fourier transform electron spin resonance. Distance measurements, Chemical Physics Letters 251 (1996) 102–110.
[6] S. Saxena, J.H. Freed, Theory of double quantum two-dimensional electron spin resonance with application to distance measurements, Journal of Chemical Physics 107 (1997) 1317–1340.
[7] G. Jeschke, M. Pannier, A. Godt, H.W. Spiess, Dipolar spectroscopy and spin alignment in electron paramagnetic resonance, Chemical Physics Letters 331 (2000) 243–252.
[8] P.P. Borbat, J.H. Freed, Multiple-quantum ESR and distance measurements, Chemical Physics Letters 313 (1999) 145–154.
[9] E. Narr, A. Godt, G. Jeschke, Selective measurements of a nitroxide–nitroxide separation of 5 nm and a nitroxide–copper separation of 2.5 nm in a terpyridine–based copper(II) complex by pulse EPR spectroscopy, Angewandte Chemie-International Edition 41 (2002) 3907–3910.
[10] I.M.C. van Amsterdam, M. Ubbink, G.W. Canters, M. Huber, Measurement of a Cu–Cu distance of 26 Å by a pulsed EPR method, Angewandte Chemie-International Edition 42 (2003) 62–64.
[11] B.E. Bode, J. Plackmeyer, T.F. Prisner, O. Schiemann, PELDOR measurements on a nitroxide-labeled Cu(II) porphyrin: orientation selection, spin-density distribution, and conformational flexibility, Journal of Physical Chemistry A 112 (2008) 5064–5073.
[12] Z. Yang, J. Becker, S. Saxena, On Cu(II)–Cu(II) distance measurements using pulsed electron double resonance, Journal of Magnetic Resonance 188 (2007) 337–343.
[13] A.V. Astashkin, J. Seravalli, S.O. Mansoorabadi, G.H. Reed, S.W. Ragsdale, Pulsed electron paramagnetic resonance experiments identify the paramagnetic intermediates in the pyruvate ferredoxin oxidoreductase catalytic cycle, Journal of the American Chemical Society 128 (2006) 3888–3889.
[14] L.J. Berliner, S.S. Eaton, G.R. Eaton, Distance Measurements in Biological Systems by EPR, Kluver Academic/Plenum Publishers, New York, 2000.
[15] S.S. Eaton, G.R. Eaton, Electron paramagnetic resonance techniques for measuring distances in proteins, Structures and Mechanisms: From Ashes to Enzymes 827 (2002) 321–339.

[16] S.S. Eaton, G.R. Eaton, Interaction of spin labels with transition metals; Part 2, Coordination Chemistry Reviews 83 (1988) 29–72.
[17] S. Lyubenova, M.K. Siddiqui, M.J.M.P. de Vries, B. Ludwig, T.F. Prisner, Protein–protein interactions studied by EPR relaxation measurements: cytochrome *c* and cytochrome *c* oxidase, Journal Physics Chemistry B 111 (2007) 3839–3846.
[18] D. Ulyanov, B.E. Bowler, G.R. Eaton, S.S. Eaton, Electron–electron distances in spin-labeled low-spin metmyoglobin variants by relaxation enhancement, Biophysical Journal 95 (2008) 5306–5316.
[19] H. Jäger, A. Koch, V. Maus, H.W. Spiess, G. Jeschke, Relaxation-based distance measurements between a nitroxide and a lanthanide spin label, Journal of Magnetic Resonance 194 (2008) 254–263.
[20] L.V. Kulik, S.A. Dzuba, I.A. Grigoryev, Y.D. Tsvetkov, Electron dipole–dipole interaction in ESEEM of nitroxide biradicals, Chemical Physics Letters 343 (2001) 315–324.
[21] L.V. Kulik, Y.A. Grishin, S.A. Dzuba, I.A. Grigoryev, S.V. Klyatskaya, S.F. Vasilevsky, Y.D. Tsvetkov, Electron dipole–dipole ESEEM in field-step ELDOR of nitroxide biradicals, Journal of Magnetic Resonance 157 (2002) 61–68.
[22] C. Albarran, J.A. Navarro, F.P. Molina-Heredia, P.S. Murdoch, M.A. De la Rosa, M. Hervas, Laser flash-induced kinetic analysis of cytochrome *f* oxidation by wild-type and mutant plastocyanin from the cyanobacterium Nostoc sp. PCC 7119, Biochemistry 44 (2005) 11601–11607.
[23] A. Abragam, B.I. Bleaney, Electron Paramagnetic Resonance of Transition Ions, Oxford University Press, New York, 1970.
[24] G.E. Pake, Nuclear resonance absorption in hydrated crystals—fine structure of the proton line, Journal of Chemical Physics 16 (1948) 327–336.
[25] A.L. Bloom, Nuclear induction in inhomogeneous fields, Physical Review 98 (1955) 1105–1111.
[26] M. Pannier, S. Veit, A. Godt, G. Jeschke, H.W. Spiess, Dead-time free measurement of dipole–dipole interactions between electron spins, Journal of Magnetic Resonance 142 (2000) 331–340.
[27] L.V. Kulik, I.A. Grigor'ev, E.S. Salnikov, S.A. Dzuba, Y.D. Tsvetkov, Electron spin-echo envelope modulation induced by slow intramolecular motion, Journal of Physical Chemistry A 107 (2003) 3692–3695.
[28] A. Savitsky, A.A. Dubinskii, M. Flores, W. Lubitz, K. Möbius, Orientation-resolving pulsed electron dipolar high-field EPR spectroscopy on disordered solids: I. Structure of spin-correlated radical pairs in bacterial photosynthetic reaction centers, Journal of Physical Chemistry B 111 (2007) 6245–6262.
[29] G. Jeschke, A. Koch, U. Jonas, A. Godt, Direct conversion of EPR dipolar time evolution data to distance distributions, Journal of Magnetic Resonance 155 (2002) 72–82.
[30] G. Jeschke, V. Chechik, P. Ionita, A. Godt, H. Zimmermann, J. Banham, C.R. Timmel, D. Hilger, H. Jung, DeerAnalysis2006—a comprehensive software package for analyzing pulsed ELDOR data, Applied Magnetic Resonance 30 (2006) 473–498.
[31] G. Jeschke, Determination of the nanostructure of polymer materials by electron paramagnetic resonance spectroscopy, Macromolecular Rapid Communications 23 (2002) 227–246.
[32] V. Schünemann, A.X. Trautwein, J. Illerhaus, W. Haehnel, Mossbauer and electron paramagnetic resonance studies of the cytochrome *b f* complex, Biochemistry 38 (1999) 8981–8991.
[33] Y. Zhou, B.E. Bowler, G.R. Eaton, S.S. Eaton, Electron spin lattice relaxation rates for $S = 1/2$ molecular species in glassy matrices or magnetically dilute solids at temperatures between 10 and 300 K, Journal of Magnetic Resonance 139 (1999) 165–174.
[34] J.L. Du, G.R. Eaton, S.S. Eaton, Temperature, orientation, and solvent dependence of electron spin–lattice relaxation rates for nitroxyl radicals in glassy solvent and doped solids, Journal of magnetic resonance, Series A 115 (1994) 213–221.
[35] A.N. Volkov, J.A.R. Worrall, E. Holtzmann, M. Ubbink, Solution structure and dynamics of the complex between cytochrome *c* and cytochrome *c* peroxidase determined by paramagnetic NMR, Proceedings of The National Academy of Sciences of The United States of America 103 (2006) 18945–18950.
[36] M.G. Finiguerra, M. Prudencio, M. Ubbink, M. Huber, Accurate long-range distance measurements in a doubly spin-labeled protein by a four-pulse, double electron–electron resonance method, Magnetic Resonance in Chemistry 46 (2008) 1096–1101.
[37] Y. Polyhach, A. Godt, C. Bauer, G. Jeschke, Spin pair geometry revealed by high-field DEER in the presence of conformational distributions, Journal of Magnetic Resonance 185 (2007) 118–129.